Available online at www.sciencedirect.com
ScienceDirect
Applied Acoustics 69 (2008) 601–613
applied acoustics
www.elsevier.com/locate/apacoust

An approximate treatment of reflection coefficient in the phased beam tracing method for the simulation of enclosed sound fields at medium frequencies

Cheol-Ho Jeong [a], Jeong-Guon Ih [a,*], Jens H. Rindel [b]

[a] *Center for Noise and Vibration Control, Department of Mechanical Engineering, Korea Advanced Institute of Science and Technology, Daejeon 305-701, Republic of Korea*
[b] *Acoustic Technology, Technical University of Denmark, Lyngby, Denmark*

Received 27 December 2006; received in revised form 4 February 2007; accepted 6 February 2007
Available online 27 March 2007

Abstract

The phased beam tracing method (PBTM) was suggested as a medium-frequency simulation technique for the calculation of impulse response, although main assumptions of geometric acoustics still hold. The phased method needs the reflection coefficient for characterizing the acoustic property of a surface and the complex wave number for describing the propagation characteristics. In this study, two types of approximate real reflection coefficients derived from the measured absorption coefficient were tested for a practical applicability. As a test example, pressure impulse responses and energy impulse responses computed from the PBTM were compared with those from the measurement and the ordinary beam tracing method. The PBTM employing the approximate reflection coefficients greatly increased the accuracy of the prediction compared to the ordinary beam tracing method, in particular at the medium-frequency range in octave bands above the Schroeder cutoff frequency. A comparison was made between angle-dependent and angle-independent reflection coefficients in the calculation of acoustic measures. Although the angle-dependent reflection coefficient yielded best matched results with measured data, but the simple angle-independent reflection coefficient can be also used with a reasonably good precision.

Keywords: Approximate reflection coefficient; Room acoustic simulation; Medium frequencies; Phased beam tracing

1. Introduction

Geometrical acoustic simulation techniques, such as ray or beam tracing method (hereafter, RTM, BTM, respectively) [1,2] and image source method [3], have been widely used to simulate the acoustic field of enclosed spaces at high frequencies. Hybrid techniques were also suggested by combining the best features of both methods [4,5]. In the RTM, it is principally assumed that the wave propagation can be described by the travel of a particle along the ray paths, which can be determined entirely by the geometrical shape of an enclosure. Because the accuracy of the simulation is related to the ratio of the wavelength to the characteristic length of the room, the sound field of a very small room is not a proper target of the geometrical acoustics method. In a practical situation for the application of RTM or BTM to the low and medium-frequency ranges, big discrepancies between simulation and measurement have been observed. This is mainly due to the fact that the conventional RTM and BTM neglect the phase information, which is essential for the analysis of interference at low and medium frequencies. The other reason of discrepancy is due to the use of statistically determined and frequency-averaged material properties of the enclosing walls, i.e., the absorption coefficient. Usually, the low frequency region can be analyzed by using the modal techniques like FEM, BEM, or FDM, but the mid frequency range still needs an appropriate method for the analysis and design.

* Corresponding author. Tel.: +82 42 869 3035; fax: +82 42 869 8220.
E-mail address: J.G.Ih@kaist.ac.kr (J.-G. Ih).

0003-682X/$ - see front matter © 2007 Elsevier Ltd. All rights reserved.
doi:10.1016/j.apacoust.2007.02.002

The phased beam tracing technique was suggested to overcome the inherent problems of energy method at mid frequencies by including the phase information in the geometrical acoustics. The application range can be extended to mid frequencies due to the improvement in the simulation accuracy. Needless to say, the realistic prediction of impulse response in an enclosure is utmost important for the auralization with three-dimensional concept or the virtual acoustic simulation. The object of the present study is to test the real valued approximate reflection coefficients of the enclosing walls for the prediction of the pressure impulse response in an enclosure. By employing a further realistic boundary condition into the phased beam tracing technique, one can approach a step closer to connect the gap between modal methods and ray tracing technique.

2. Treatment of wall absorption

2.1. Phased beam tracing method (PBTM)

The results of the ray or beam tracing method rely greatly on the number of rays (or beams) and receiver size. There were some previous works on the determination of receiver size (for example [6–8]). Beams should densely cover the space to describe the propagation of spherical wave adequately. To this end, the triangular beam tracing method [2,9–11] can be employed to avoid the use of complicated weighting functions for resolving the overlapping problem of cone tracing method [12].

In the conventional beam tracing method, beams carry the energy quantity. Emitted beam possesses some amount of energy at the starting point and, during the propagation within the enclosure, it loses a part of initial energy owing to the air attenuation and the absorption at the hitting surfaces. As a result, energy reflectogram (or echogram) for a frequency band can be found using the arrival time of a beam and the energy at that time at the observer point.

Apart from the conventional beam tracing method, there exist two types of the phased geometrical acoustics methods; one is the phased ray or beam tracing method and the other is the phased image source method. The first attempt for phased ray tracing method was made by Geest and Patzold [13]. An extended study on this matter was conducted by Shin and Ih [10] including a study on the diffraction effect. The precision of the method in the low and high frequency limits was compared with the boundary element method (BEM) and measurement. For the phased image source method, Dance et al. [14] attempted to describe the interference effect including phase. Suh and Nelson [15] simulated the impulse response and frequency response function using the phase image model. Improvement in prediction was achieved by applying the measured complex impedance to the reflection at the wall. Using a similar method, Zeng et al. [16] also calculated the reverberation time and sound level, which agreed with measured data.

Complex numbers are involved in the simulation by the phased method. They are reflection coefficients and the wave number representing the acoustical properties of the surfaces, and the phase change during the propagation and the attenuation in the air, respectively. Because the pressure impulse response is preferred as the final target function of the room acoustic simulation rather than the energy reflectogram, the phase information should be retained. Pressure reflection coefficient, $r(\theta)$, characterizes

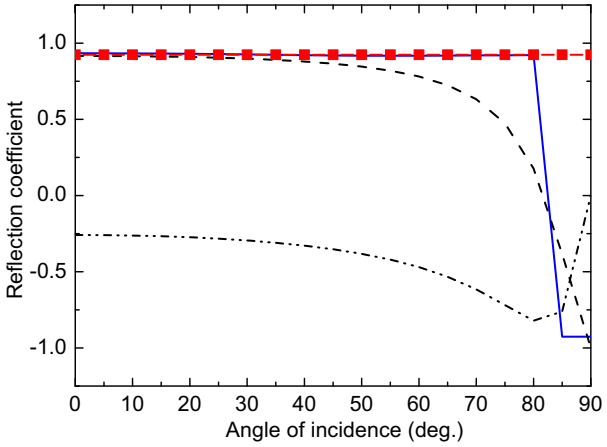

Fig. 1. A comparison of measured and approximated (i.e., real valued) reflection coefficients, r^{i}_{θ} and r^{d}_{θ}, as a function of incidence angle (200 Hz): (- - -) real part of the measured reflection coefficient r; (-·-·-) imaginary part of the measured r; (–■–) angle-independent real reflection coefficient r^{i}_{θ}; (—) angle-dependent real reflection coefficient r^{d}_{θ}. The test sample was 20 mm-thick PU form (*surface impedance* $Z_w = 511–2881\,j$, absorption coefficient $\alpha_s = 0.15$ at 200 Hz).

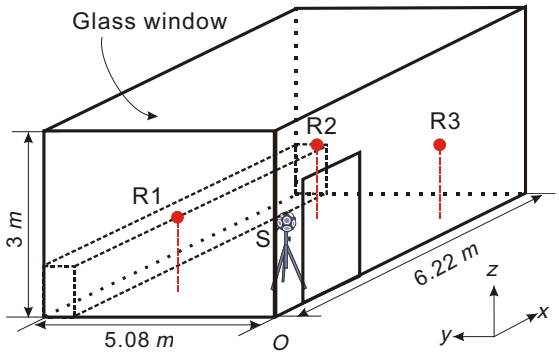

Fig. 2. Geometry and dimensions of the test room. S (1.5, 1.5, 1.1) indicates the position of the source and R1 (1.5, 3.08, 1.27), R2 (4.72, 3.58, 1.27), R3 (4.72, 1.5, 1.27) are the receiver points.

Table 1
Absorption coefficients of the test room surfaces

Surface and material	Octave-band center frequencies (Hz)			
	125	250	500	1k
Wooden floor	0.15	0.12	0.11	0.10
Absorptive ceiling	0.60	0.72	0.78	0.82
Brick wall	0.01	0.02	0.03	0.04
Glass window	0.10	0.08	0.05	0.04
Gypsum wall	0.15	0.11	0.08	0.08
Ventilation grating	0.40	0.50	0.50	0.60

not only the magnitude change at the surface, but also the phase shift. When diffraction and scattering effects are assumed to be negligible and only the geometrical law of reflection is considered, the pressure at a receiver can be expressed as

$$p(t = a_{\text{tot}}/c) = \frac{p_0}{a_{\text{tot}}} \mathrm{e}^{-\mathrm{j}\widetilde{k}a_{\text{tot}}} \prod_{i=1}^{n} r_i(\theta_i), \tag{1}$$

where p_0 is the initial pressure amplitude, a_{tot} the total travel distance of a beam, $\widetilde{k}$ the complex wave number

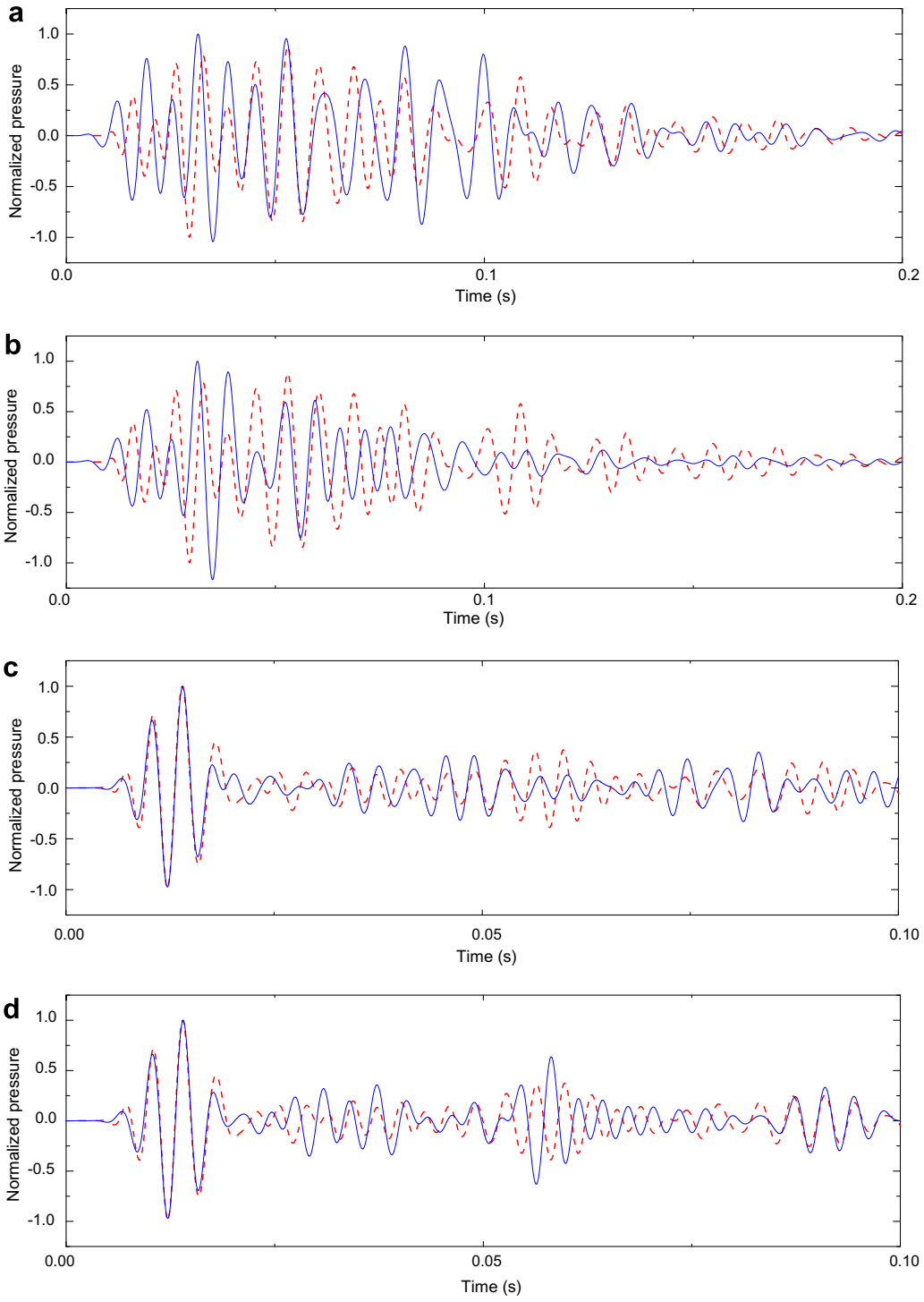

Fig. 3. A comparison of measured and calculated pressure impulse responses at a receiver position R1: (---) measured; (—) calculated by the PBTM. (a), (b) 125 Hz; (c), (d) 250 Hz; (e), (f) 500 Hz; (g), (h) 1 kHz. (a), (c), (e), (g) Use of angle-independent reflection coefficient r_{θ}^{i}; (b), (d), (f), (h) use of angle-dependent reflection coefficient r_{θ}^{d}.

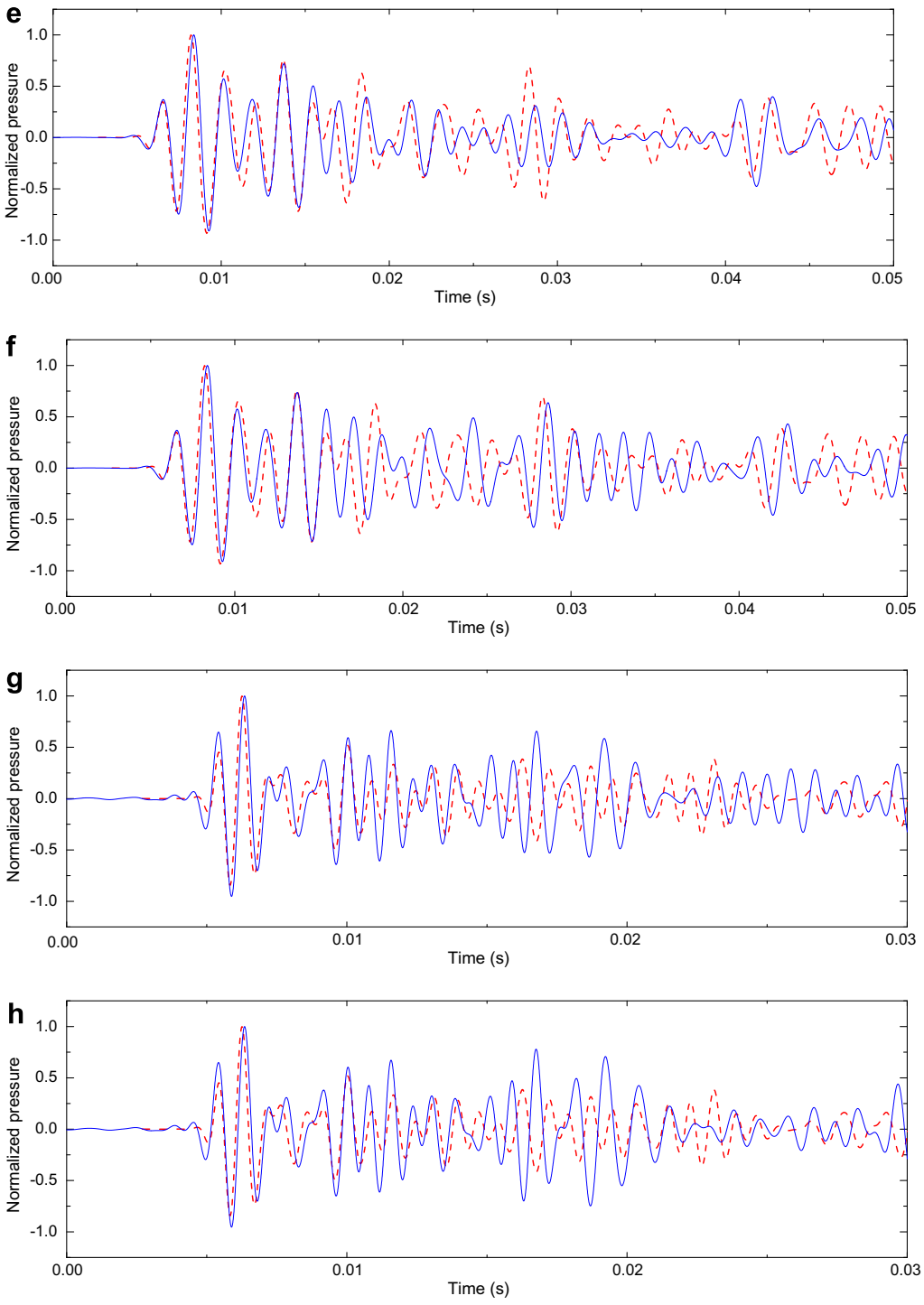

Fig. 3 *(continued)*

($\widetilde{k} = k - \mathrm{j}m/2$), k the wave number in the lossless free field, m the air attenuation factor, $r_i(\theta_i)$ the pressure reflection coefficient of the ith reflection, and θ_i the angle of incidence of the beam, n the total number of reflections. Once the pressure reflectogram is found for a frequency, the steady-state response can be obtained simply by the summation of direct sound and successive transient components. If the steady-state pressures are computed for all frequencies within the frequency range of interest, steady-state transfer function can be constructed. In this procedure, the information on the arrival time will be discarded. One can use the steady-state transfer function to obtain an impulse response by taking the inverse Fourier transform.

Although the applicable frequency range for geometrical acoustics is not clearly given yet, one might use the Schroeder cutoff frequency [17], f_c, as a demarcation distinguishing *high* frequency range from *low* frequency range. Above the Schroeder frequency, it is supposed that there

are at least three modes within the half-power bandwidth of the frequency band (preferably, 1/3-octave band) of interest. Beyond f_c, the space can be assumed as a reverberant sound field in a statistical sense. Sometimes, the frequency range is categorized into three areas using f_c [10,18]: low, mid, and high frequency. The medium-frequency range is defined in between f_c and $4f_c$, and one can apply the phased geometrical acoustics technique very well in this range. At high frequencies over $4f_c$, the wavelength is small enough to apply the geometrical or statistical acoustics technique. Shin and Ih [10] have shown that the applicable frequency range of the phased beam tracing technique can be extended to low and high frequencies outside the aforementioned mid-frequency range with accepting small errors.

2.2. Reflection coefficient

For the implementation of the PBTM, the reflection coefficients of walls should be known; in fact, it can be easily calculated from the measured surface impedance, if the data is available. For the practical purpose, in particular in the initial design stage, the reflection coefficient can be approximately deduced from the absorption coefficient with some assumptions. As a rough assumption, one can employ the real-valued reflection coefficient and the locally reacting surface. Then, the reflection coefficient simply becomes the 'angle-independent', real reflection coefficient, r_θ^{i}, expressed as $r_\theta^{\mathrm{i}} = \pm\sqrt{1-\alpha_{\mathrm{s}}}$. Here, α_{s} denotes the statistical absorption coefficient of the surface material under diffuse condition. Acoustically hard material is associated with the positive sign, whereas the negative value stands for the acoustically soft material.

Alternatively, an 'angle-dependent' reflection coefficient, r_θ^{d}, can be also used approximately, which is obtained using the surface impedance and the radiation impedance as follows: [19]

$$r_\theta^{\mathrm{d}} = \frac{Z_{\mathrm{w}} - Z_{\mathrm{r}}(\theta)}{Z_{\mathrm{w}} + Z_{\mathrm{r}}(\theta)}. \tag{2}$$

Here, Z_{w} means the surface impedance of the wall and Z_{r} the radiation impedance. The surface impedance can be calculated again from the angle-independent reflection coefficient, r_θ^{i}, and the equivalent radiation impedance Z_{r}^* of the wall material, expressed as $Z_{\mathrm{w}} = Z_{\mathrm{r}}^* \frac{1+r_\theta^{\mathrm{i}}}{1-r_\theta^{\mathrm{i}}}$. Equivalent radiation impedance is a compensation factor to match the random incidence absorption coefficient, obtained from the real reflection coefficient, with the initially given absorption coefficient, α_{s}. For finite surfaces, $Z_{\mathrm{r}}^*/\rho c$ is smaller than 1.64 and it depends on ke, in which e denotes the characteristic dimension expressed as $e = 4S/U$, S is the

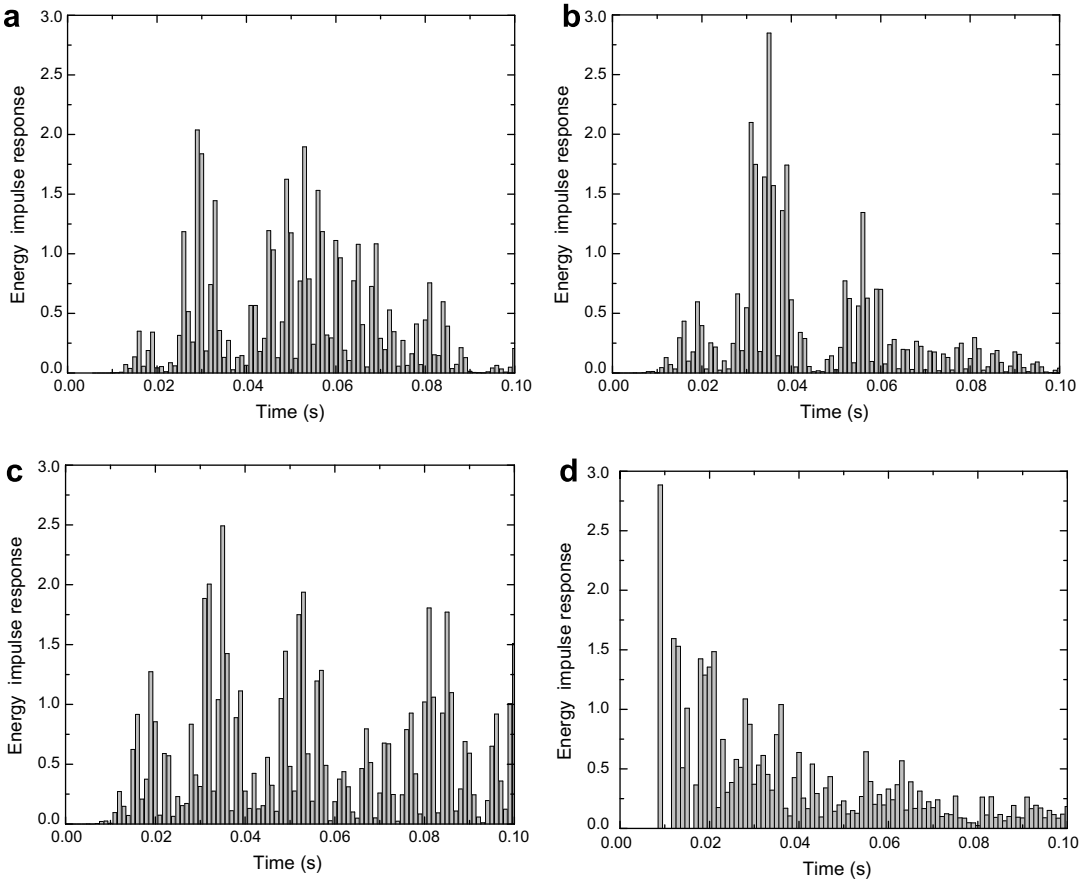

Fig. 4. A comparison of measured and calculated energy impulse responses at 125 Hz (R1 position). (a) Measurement, (b) PBTM using r_θ^{d}, (c) PBTM using r_θ^{i}, (d) BTM.

area, and U the perimeter. An approximated solution for Z_r in Eq. (2) is given by [19]

$$Z_r = \rho c \left[\left(\cos^2\theta - A\frac{2\pi}{ke} \right)^2 + B\left(A\frac{2\pi}{ke} \right)^2 + \left(\frac{2\pi}{(ke)^2} \right)^4 \right]^{-\frac{1}{4}}, \tag{3}$$

where the empirical constants A and B are 0.6 and π, respectively, obtained by trial and fitting method. One can note that the size effect is included in the definition of r_θ^d. Approximate radiation impedance, Z_r, in Eq. (3) differs from the numerical results within $\pm 10\%$ for $ke > 8$ and up to $\pm 20\%$ for $ke < 8$ [19]. Fig. 1 shows a comparison between measured reflection coefficient, r, and approximated reflection coefficients. Naturally, the angle-independent reflection coefficient, r_θ^i, has a constant value for a given absorption coefficient. The angle-dependent reflection coefficient, r_θ^d, has both positive and negative values depending on the incidence angle. Although an abrupt change exists around 80° from positive to negative value, it corresponds better with the measured complex reflection coefficient. When the sound is incident from the almost grazing angle onto a soft material, the negative reflection coefficient can be observed [20]. Here, acoustically soft material or pressure-release boundary means that its surface impedance is sufficiently smaller than the radiation impedance, e.g., porous materials at high frequencies. The negative reflection coefficient is important in accounting for the interference effect and it can be described by r_θ^d.

3. Test example

A medium sized room with known absorption data was taken as a test example. Room dimensions were $6.22 \times 5.08 \times 3.00\ \mathrm{m}^3$ as shown in Fig. 2. The wall absorption coefficient data are as listed in Table 1. A wall having a door and another wall in yz-plane at $(6.22, y, z)$ were brick walls and a wall in yz-plane at $(0, y, z)$ had a plaster surface. The upper space of the wall in xz-plane at $(x, 5.08, z)$ is made of glass. Source (S) and receiver (R1) were located at (1.50 m, 1.50 m, 1.10 m) and (1.50 m, 3.08 m, 1.27 m), respectively. The height of R1 position corresponded with a human sitting posture. Measurement and analysis of impulse response were conducted according to the ISO 3382 standard [21]. The maximum length sequence (MLS) signal was radiated from a dodecahedron omni-directional source and the transmitted sound was picked up using an omni-directional microphone (AKG C34).

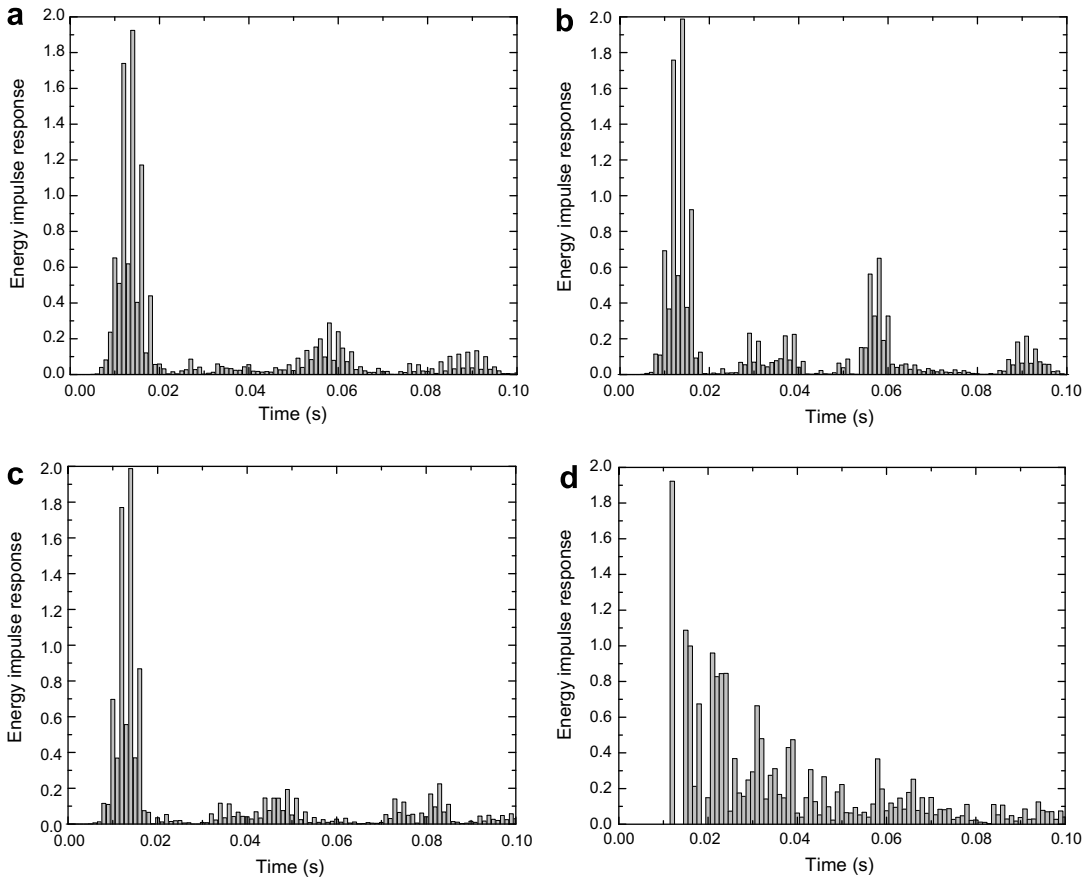

Fig. 5. A comparison of measured and calculated energy impulse responses at 250 Hz (R1 position). (a) Measurement, (b) PBTM using r_θ^d, (c) PBTM using r_θ^i, (d) BTM.

The Schroeder cutoff frequency, f_c, of this room was calculated as 150 Hz; therefore, it is expected that the PBTM will be useful within the medium-frequency range of 150–600 Hz. Because the absorption at the ceiling (acoustic tile) was large, the reflection in between the ceiling and floor was much weaker than other directional reflections. In the simulation, the number of beams was 2000 and the number of reflections was allowed up to 30 to obtain the impulse response of 1 s in duration. Both of r_θ^i and r_θ^d concepts were tested. One should remind that r_θ^d also takes the size effect of the reflecting surfaces into account.

The early parts of pressure impulse responses for octave bands in the range of 125 Hz–1 kHz are shown in Fig. 3. It should be recalled that 125 Hz band is lower than f_c and 1 kHz band is higher than $4f_c$; the frequency span in between two bands can be called the medium-frequency range. The displayed time lengths of the impulse responses were halved with increasing the frequency by an octave to clearly demonstrate the similarity of wave forms. The predicted impulse response at 125 Hz shows some differences with the measurement. One can find that an excessive decay in the late part is introduced by employing r_θ^d. At 250 Hz, both simulations employing r_θ^i and r_θ^d show excellent correspondence with measurement. Predicted direct sound from source to receiver, which is not affected by any reflection from the wall, matches exactly with measured data. The peaks are slightly overestimated using r_θ^d, but the overall trend of the transient response is more similar to the measured response than the case using r_θ^i. When r_θ^d is employed in the simulation at 500 Hz band, a precise prediction of responses around 0.03 s was obtained in contrast to the case using r_θ^i. The overall trend of predicted impulse response corresponds to the measured data very well. In the simulation at 1 kHz band, a reasonable agreement with measurement can be seen although the frequency band exceeds the high frequency limit of applicable range. The predicted peak values of the angle-dependent case are slightly bigger than those of angle-independent case. The simulation results as shown in Fig. 3 reveal that the PBTM using real reflection coefficient can be a very useful mid frequency predictor for the pressure impulse response in an enclosed room. One can also find a possibility for the extension of the applicable range at low and high frequency ends, if some error can be accepted in an engineering sense.

The pressure impulse response cannot be obtained from the beam tracing method. Therefore, energy impulse responses, which can be obtained by squaring a pressure impulse response, computed from BTM and PBTM were compared with the measured data as shown in Figs. 4–7, for 125 Hz, 250 Hz, 500 Hz, and 1 kHz band, respectively.

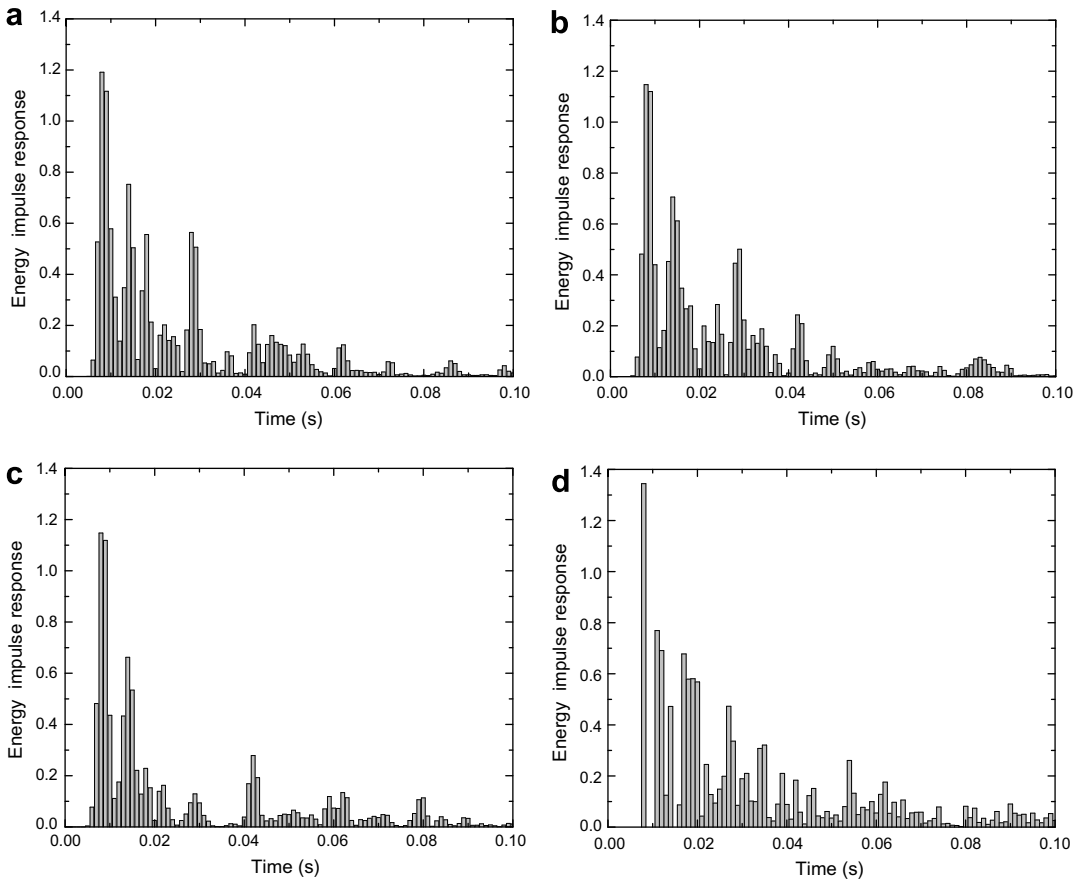

Fig. 6. A comparison of measured and calculated energy impulse responses at 500 Hz (R1 position). (a) Measurement, (b) PBTM using r_θ^d, (c) PBTM using r_θ^i, (d) BTM.

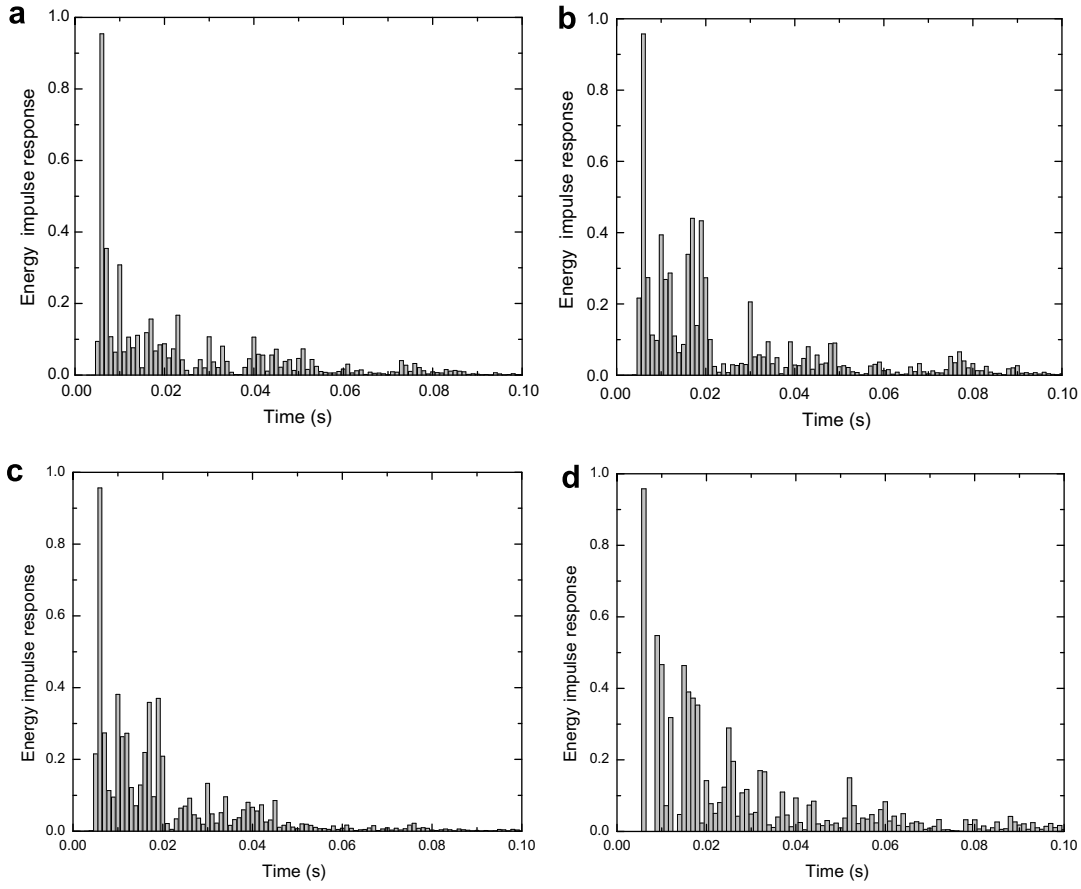

Fig. 7. A comparison of measured and calculated energy impulse responses at 1 kHz (R1 position). (a) Measurement, (b) PBTM using r_θ^d, (c) PBTM using r_θ^i, (d) BTM.

Significant differences can be observed between PBTM and BTM results. The predicted energy impulse responses by using BTM usually show monotonic decay, because energy of the reflected beam is smaller than that of a direct sound. The results by using PBTM show a good agreement with measured data, especially when r_θ^d is used. It is noted that the predicted energy impulse responses by using both methods become similar at 1 kHz, which is beyond $4f_c$.

Reverberation times (early decay time, EDT; T30), Definition (D50, D80), Clarity (C80), and center time (Ts) [21] were calculated from the simulated and measured impulse responses. In estimating EDT, the PBTM using r_θ^d yields an excellent agreement with measured data, whereas the other predictions seem to be slightly different as shown in Table 2. This means that the initial part of impulse response is accurately predicted by employing the PBTM, which clearly show the angle-dependent acoustic characteristics of walls. In the results of T30 and D50 calculations, both BTM and PBTM show good agreements with measured data. It is noted that the predicted parameters agree well with measured data, although the energy impulse response by using the BTM is clearly different. D80 data shows a distinguishable difference between BTM and PBTM. D80 by using BTM is underestimated regardless of frequency while D80 values by using PBTM show a good agreement irrespective of the types of reflection coef-

Table 2
A comparison of measured and calculated room acoustic measures (R1)

Acoustic measures	Frequency (Hz)	Measured	PBTM, r_θ^d	PBTM, r_θ^i	BTM
EDT (s)	125	0.58	0.50	0.70	0.69
	250	0.56	0.56	0.62	0.61
	500	0.47	0.44	0.46	0.63
	1k	0.38	0.37	0.27	0.46
T30 (s)	125	0.87	0.70	0.77	0.70
	250	0.58	0.60	0.54	0.62
	500	0. 60	0.63	0.61	0.64
	1k	0.58	0.59	0.54	0.50
D50	125	0.64	0.80	0.53	0.77
	250	0.77	0.79	0.77	0.78
	500	0.84	0.85	0.81	0.78
	1k	0.88	0.88	0.92	0.84
D80	125	0.82	0.91	0.81	0.87
	250	0.89	0.88	0.90	0.84
	500	0.90	0.93	0.95	0.84
	1k	0.95	0.96	0.97	0.91
C80 (dB)	125	6.7	11.5	6.3	9.1
	250	9.1	8.7	9.6	7.2
	500	9.3	11.0	12.7	7.2
	1k	12.4	13.5	14.6	9.8
Ts (ms)	125	50.1	39.7	51.6	47.4
	250	28.2	30.7	28.1	32.2
	500	28.1	24.9	28.1	32.6
	1k	22.9	24.9	20.1	25.1

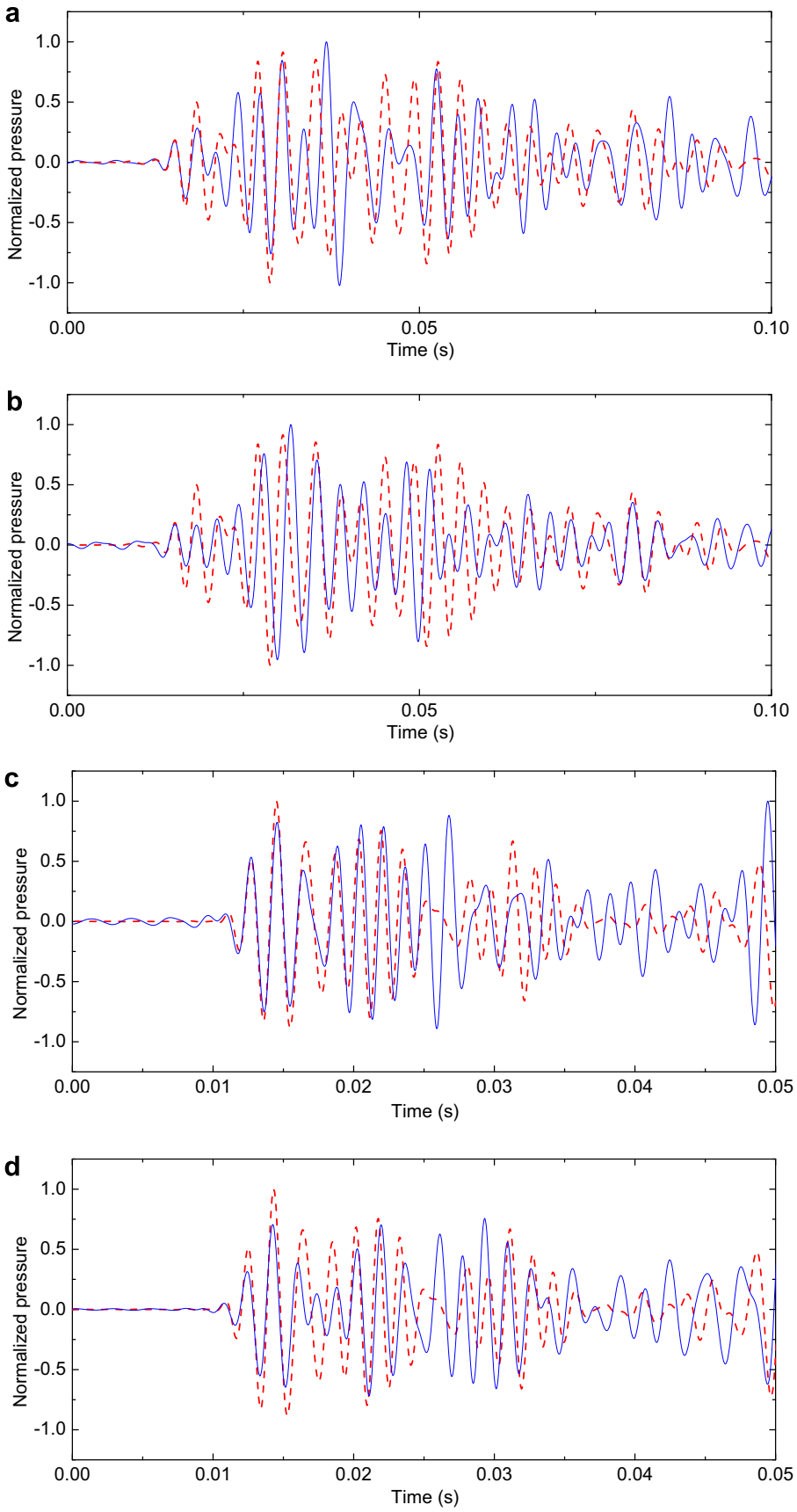

Fig. 8. A comparison of measured and calculated pressure impulse responses (R2 position): (---) measured; (—) calculated by PBTM. (a), (b) 250 Hz; (c), (d) 500 Hz. (a), (c) Use of angle-independent reflection coefficient r_{θ}^{i}; (b), (d) use of angle-dependent reflection coefficient r_{θ}^{d}.

Table 3
A comparison of measured and calculated room acoustic measures (R2)

Acoustic measures	Frequency (Hz)	Measured	PBTM, r_θ^d	PBTM, r_θ^i	BTM
EDT (s)	125	0.65	0.42	0.71	0.64
	250	0.51	0.51	0.51	0.52
	500	0.69	0.54	0.64	0.52
	1k	0.41	0.47	0.52	0.44
T30 (s)	125	0.85	0.64	0.79	0.65
	250	0.73	0.71	0.63	0.60
	500	0.62	0.56	0.60	0.60
	1k	0.66	0.57	0.64	0.57
D50	125	0.59	0.73	0.61	0.71
	250	0.79	0.83	0.68	0.80
	500	0.70	0.77	0.78	0.80
	1k	0.84	0.85	0.85	0.84
D80	125	0.82	0.84	0.85	0.83
	250	0.88	0.92	0.79	0.90
	500	0.83	0.86	0.87	0.90
	1k	0.93	0.94	0.94	0.92
C80 (dB)	125	6.5	7.1	7.2	7.1
	250	8.5	10.6	7.0	9.7
	500	7.0	8.1	8.5	9.7
	1k	11.2	12.1	12.7	10.6
Ts (ms)	125	51.5	45.7	50.8	41.8
	250	41.5	36.0	57.6	30.5
	500	38.2	39.6	37.2	29.8
	1k	28.7	28.9	24.7	26.7

ficient. Similarly, in C80, one can clearly observe that the PBTM result shows better correspondence with measurement. Results by using BTM are underestimated because of the reverberation after 80 ms, while the measured data and PBTM results display little reverberation components in Figs. 5 and 6. It is hard to predict the Ts, because the overall shape of the predicted transient response should correspond well with the measured data. The predicted data by PBTM are smaller than the measured data due to a small overestimation in the early part before 20 ms at 500 Hz and 1 kHz bands, while the BTM prediction yields an overestimated data.

The other two receiver positions, R2 (4.72 m, 3.58 m, 1.27 m) and R3 (4.72 m, 1.5 m, 1.27 m) as shown in Fig. 2, were also tested. These two additional points have the same height as the former receiving position, R1. Because the main purpose of this paper was to test a new method for the prediction of the impulse response more precisely than before, the study was focused on the human hearing position in the chamber, thus the receiver height was determined as 1.27 m in a sitting posture. The three receiving points were selected to have some meaning, though. R1 was a point near to the source and near to the *yz*-plane; R2 was a point far from the source in a diagonal way and it is very near to the glass window in *xz*-plane; R3 was a point far from the source and its distance from the *xz*-plane was the same with the source point, which was located at a nearly symmetric position in *x*-direction. One-dimensional reflections along *x*- and *y*-direction should have been dominant at R3 and R1, respectively, whereas the result at R2 was not strongly influenced by such one-dimensional reflection. In Fig. 8, the measured and calculated pressure impulse responses at R2 in medium frequencies are shown. The peaks in the pressure impulse response are slightly shifted in the early parts of the impulse response due to the incorrect phase shift at the wall by employing the real reflection coefficient and some diffraction effect near the HVAC system than other receiving points. Table 3 shows a comparison of measured and calculated acoustic parameters at R2. All simulation results, including the data calculated in 1 kHz octave band which can be considered as high frequency, show a reasonable agreement with measurement. It is noted that the center times using the BTM were clearly smaller than the measured data. This was resulted from the monotonic decaying characteristic of BTM result. In 250 Hz and 500 Hz bands, the calculated center times using the PBTM were larger than those calculated by using the BTM and they correspond better with measured data than the BTM.

Fig. 9 and Table 4 show the comparisons of pressure impulse response and acoustic parameters at R3. In Fig. 9, calculation method using r_θ^d yielded better results than using r_θ^i, especially in 500 Hz octave band. Also, C80 and center times computed from the PBTM at medium frequencies corresponded better with measured data.

It is also noted at R2 and R3 positions that many acoustic parameters obtained by PBTM using the angle-dependent reflection coefficient agreed with measured data very closely even at 125 Hz, which is lower than the Schroeder cutoff frequency; however, large differences can be seen at R1 position and some parameters at R2 and R3 positions at 125 Hz. At 1 kHz which is higher than the high frequency limit of PBTM application, it is observed that all acoustic parameters obtained by PBTM using the angle-dependent reflection coefficient agreed very closely with measured data compared to the BTM, except EDT, T30 only at R3 position.

The computation time was about 10 minutes in using the angle-independent reflection coefficient r_θ^i for the calculation of transfer function, impulse response, and acoustic parameters (executed on a 3 GHz Intel Pentium 4 PC with 1 GB RAM). For the same calculations, it took about 5 hours in using the angle-dependent reflection coefficient r_θ^d. Additional time for calculating incidence angle and radiation impedance was required when r_θ^d was employed. The computation time consists of time for tracing the triangular beams and calculating the transfer function. Definitely, the calculation time mostly depends on the number of reflections and the frequency resolution (in this case, the frequency resolution was 0.5 Hz). In both cases, the computation time for beam tracing and receiver detection was commonly 55 s for the test model. Excluding this common treatment time, 1 s was consumed for each frequency calculation in using r_θ^i, while 31 s used in using r_θ^d.

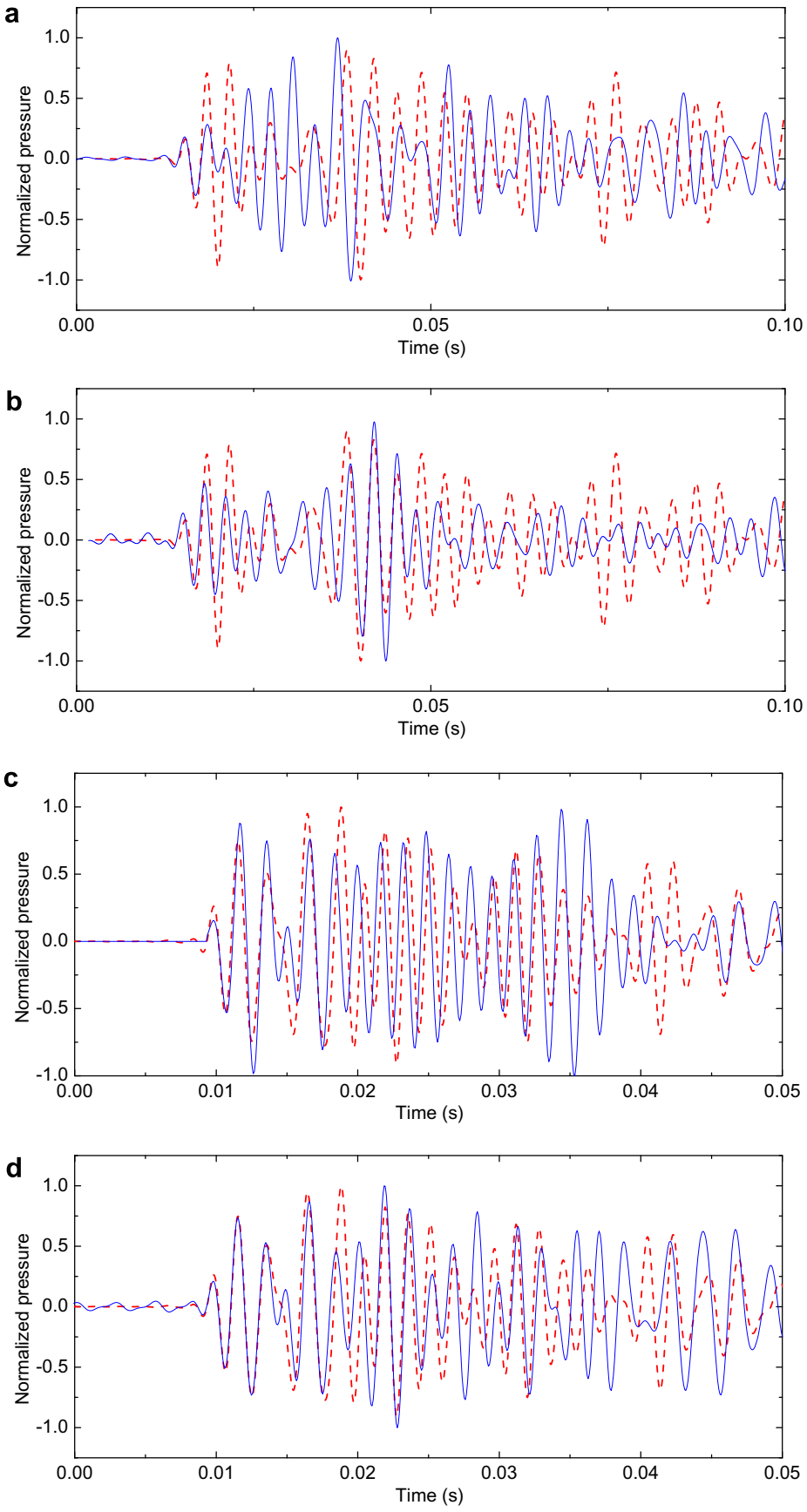

Fig. 9. A comparison of measured and calculated pressure impulse responses (R3 position): (---) measured; (—) calculated by PBTM. (a), (b) 250 Hz; (c), (d) 500 Hz. (a), (c) Use of angle-independent reflection coefficient r_θ^i; (b), (d) use of angle-dependent reflection coefficient r_θ^d.

Table 4
A comparison of measured and calculated room acoustic measures (R3)

Acoustic measures	Frequency (Hz)	Measured	PBTM, r_θ^d	PBTM, r_θ^i	BTM
EDT (s)	125	0.43	0.46	0.59	0.63
	250	0.57	0.54	0.59	0.50
	500	0.56	0.57	0.57	0.50
	1k	0.38	0.51	0.43	0.42
T30 (s)	125	0.83	0.29	0.85	0.65
	250	0.73	0.61	0.77	0.60
	500	0.59	0.64	0.59	0.60
	1k	0.69	0.29	0.67	0.56
D50	125	0.87	0.86	0.72	0.70
	250	0.65	0.74	0.50	0.80
	500	0.75	0.74	0.71	0.80
	1k	0.86	0.82	0.78	0.84
D80	125	0.92	0.92	0.88	0.84
	250	0.87	0.84	0.80	0.90
	500	0.89	0.87	0.87	0.90
	1k	0.95	0.94	0.95	0.93
C80 (dB)	125	10.7	10.3	8.9	7.2
	250	8.2	7.2	6.6	9.9
	500	8.9	8.7	8.2	10.0
	1k	12.4	12.1	12.8	11.0
Ts (ms)	125	35.4	33.6	41.6	40.6
	250	46.0	49.9	55.1	29.3
	500	34.9	39.2	39.2	28.5
	1k	28.2	28.8	29.4	25.3

Each octave band response can be estimated separately by computing the transfer function in each octave band. For example, if one wants to calculate the response in 250 Hz octave band, it is possible by just computing the transfer function within a frequency range of 177–355 Hz and taking the inverse Fourier transform to obtain the impulse response of 250 Hz band. The frequency span should be larger than the half-power bandwidth of the 250 Hz octave band.

4. Conclusions

Two real-valued reflection coefficients, which were angle-dependent and angle-independent, were tested for the simulation of room acoustics at medium-frequency range. To this end, the phased beam tracing method was applied to a medium sized enclosed room to predict impulse responses and the results were compared with those of the ordinary beam tracing method. The energy impulse response by using the PBTM showed a notable improvement over the BTM, particularly in the early part of impulse response, at the mid-frequency range. Angle-dependent reflection coefficient seemed slightly better than the angle-independent one in most cases, but the difference was not very distinguished. Apparently, use of the complex reflection coefficient will improve the precision of the result, if a precisely measured data set for all surfaces were available.

The data for the three representative receiving points at sitting posture were dealt with because they could already show some tangible results. We think that it will be also very interesting to see some simulation results at a central position, points having different heights, a corner, a position in the very vicinity of the surface, etc. and further investigation on these points are needed. Also, a test on a disproportionate room will be interesting because it can readily spotlight the influence of angle-dependent reflection coefficient. However, this study clearly suggested a good possibility to use the real reflection coefficients in the simulation of the enclosed field in the medium-frequency range, notwithstanding the fact that the real reflection coefficients can not fully represent the correct phase shift on the reflection.

Acknowledgements

This work was partially supported by the BK21, the Korea Science and Engineering Foundation (KOSEF) through the National Research Lab. Program by the Ministry of Science and Technology (M10500000112-05J0000-11210), and the Korea Research Foundation (KRF) through the International Collaboration Program by the Ministry of Science and Technology (M07-2004-000-10135-0).

References

[1] Krokstad A, Stroem S, Soersdal S. Calculating the acoustical room response by the use of a ray tracing technique. J Sound Vib 1968;8:118–25.
[2] Lewers T. A combined beam tracing and radiant exchange computer-model of room acoustics. Appl Acoust 1993;38:161–78.
[3] Allen JB, Berkley DA. Image method for efficiently simulating small-room acoustics. J Acoust Soc Am 1979;65:943–50.
[4] Rindel JH. Computer simulation techniques for acoustical design of rooms. Acoust Aust 1995;23:81–6.
[5] Vorlander M. Simulation of the transient and steady-state sound propagation in rooms using a new combined ray-tracing/image-source algorithm. J Acoust Soc Am 1989;86:172–8.
[6] Lehnert H. Systematic-errors of the ray-tracing algorithm. Appl Acoust 1993;38:207–21.
[7] Zeng XY, Chen KA, Sun JC. On the accuracy of the ray-tracing algorithms based on various sound receiver models. Appl Acoust 2003;64:433–41.
[8] Yang LN, Shield BM. Development of a ray tracing computer model for the prediction of the sound field in long enclosures. J Sound Vib 2000;229:133–46.
[9] Stephenson UM. Quantized pyramidal beam tracing – a new algorithm for room acoustics and noise immission prognosis. Acustica 1996;82:517–25.
[10] Shin H-C, Ih J-G. Acoustic analysis of interior spaces by using the phased geometric acoustic model. J Acoust Soc Korea 1998;17:54–61 [in Korean].
[11] Funkhouser T, Tsingos N, Carlbom I, Elko G, Sondhi M, West JE, et al. A beam tracing method for interactive architectural acoustics. J Acoust Soc Am 2004;115:739–56.
[12] Maercke D, Martin J. The prediction of echograms and impulse responses within the epidaure software. Appl Acoust 1993;38:93–114.
[13] Geest ED, Patzold H. Comparison between room transmission functions calculated with a boundary element method and a ray tracing method including phase. In: Proceedings of internoise 96; 1996. p. 3177–80.

[14] Dance SM, Roberts JP, Shield BM. Computer-prediction of sound distribution in enclosed spaces using an interference pressure model. Appl Acoust 1995;44:53–65.
[15] Suh JS, Nelson PA. Measurement of transient response of rooms and comparison with geometrical acoustic models. J Acoust Soc Am 1999;105:2304–17.
[16] Zeng XY, Chen KA, Sun JC. Modeling the sound fields in rooms with multiple sources using a hybrid image method including phase. Acta Acust 2002;88:88–92.
[17] Schroeder MR, Kuttruff KH. On frequency response curves in rooms: comparison of experimental, theoretical, and Monte Carlo results for the average frequency spacing between maxima. J Acoust Soc Am 1962;34:76–80.
[18] Kuttruff H. Sound fields in small rooms. In: Proceedings of 15th AES; 1998. p. 11–15.
[19] Rindel JH. Modeling the angle-dependent pressure reflection factor. Appl Acoust 1993;38:223–34.
[20] Attenborough K. Review of ground effects on outdoor sound propagation from continuous broadband source. Appl Acoust 1988;24:289–319.
[21] Anon. ISO 3382. Acoustics – measurement of reverberation time of rooms with reference to other acoustical parameters; 1997.